JOURNAL OF THEORETICAL AND APPLIED MECHANICS
48, 3, pp. 771-788, Warsaw 2010

CO-ROTATIONAL FORMULATION OF A SOLID-SHELL ELEMENT UTILIZING THE ANS AND EAS METHODS

Cengiz Polat

Faculty of Engineering, Department of Civil Engineering, Firat University, Elazig, Turkey
e-mail: cpolat@firat.edu.tr

An efficient eight-node solid-shell element is demonstrated. The Assumed Natural Strain (ANS) and the Enhanced Assumed Strain (EAS) methods are used to alleviate the locking problems. A co-rotational formulation is adopted in the description, thus geometric nonlinearity is taken into account by rotation of the local coordinate system. Several benchmark problems are examined to demonstrate the efficiency of the element.

Key words: solid-shell element, co-rotational formulation, ANS-EAS method

1. Introduction

In the linear analysis, displacements and strains developed in a structure are small. That is, the geometry of the structure assumed remains unchanged during the loading process and linear strain approximations can be used. However, the geometry of the structure changes continuously during the loading process, and this fact is taken into account in geometrically nonlinear analysis. Mainly, three Lagrangian kinematic descriptions are in the present use for finite element analysis of geometrically nonlinear structures: Total Lagrangian (TL), Updated Lagrangian (UL) and Co-Rotational (CR) formulation (Felippa and Haugen, 2005). The pioneers of the co-rotational approach can be said as Wempner (1969), Argyris *et al.* (1979), Belytschko and Glaum (1979), Crisfield and Moita (1996) and Moita and Crisfield (1966). The attractiveness of the CR formulation resides in the fact that it can be applied to simplify the Lagrangian formulations for large-displacement and small-strain problems without significant loss of accuracy (Urthaler and Reddy, 2005). In this formulation, rigid-body motion is eliminated and only element deformation is considered to obtain internal forces and the tangent stiffness matrix.

Many researchers (Harnau and Schweizerhof, 2002; Hauptmann and Schweizerhof, 1998; Hauptmann etal, 2000; Miehe, 1998; Souza *et al.*, 2006; Sze and Yao, 2000; Sze *et al.*, 2000; Vu-Quoc and Tan, 2003; Zienkiewicz *et al.*, 1971) are interested in solid-shell elements which are widely used to analyze shell-like structures. These elements possess no rotational degrees-of-freedom. Thus, the complication on handling finite rotational increments can be avoided. However, similar to degenerated shell elements, these elements also suffer from some kind of locking effects. Various methods have been suggested to overcome these locking effects. The earliest techniques are Uniform Reduced Integration (URI) (Zienkiewicz *et al.*, 1971) and Selective Reduced Integration (SRI) (Hughes *et al.*, 1977, 1978). However, the URI procedure generally leads to spurious zero energy modes, despite the fact that for some cases the correct solution is obtained. In addition, the SRI procedure exhibits similar problems but usually on a smaller scale. Recently, Panasz and Wisniewski (2008) developed two nine-node shell elements by using the SRI procedure successfully. Another two distinct approaches are the Assumed Natural Strain (ANS) (Bathe and Dvorkin, 1986; Bucalem and Bathe, 1993) and the Enhanced Assumed Strain (EAS) (Andelfinger and Ramm, 1993; Klinkel and Wagner, 1997; Simo and Rifai, 1990) which are successfully implemented in various finite elements to alleviate locking effects.

The objective of this paper is to demonstrate the nearly locking free formulation of an 8-node solid-shell element based on the co-rotational description of motion. Firstly, the geometry and the strain-displacement relations of the displacement based 8-node solid-shell element are presented. Low order elements based on the standard displacement interpolation are usually accompanied by locking phenomena. To alleviate the transverse shear and trapezoidal locking problems of the element, the ANS approach is used. In addition, membrane and thickness locking treatments are done by the EAS method. The EAS method is based on the enhancing of the displacement-dependent strain field by an extra assumed strain field, and it is assumed that the stress and the enhanced assumed strain fields are orthogonal, which results in elimination of the stress field from the finite element equations. Secondly, the co-rotational formulation based on the study of Crisfield and Moita (1996), Moita and Crisfield (1996), Felippa and Haugen (2005) is given. The local coordinate system is attached to the element and a rotation matrix, which defines the rotation of this local coordinate system according to the global coordinate system, is obtained using the polar decomposition theorem. Thus, the geometric non-linearity is incorporated by the rotation of the local coordinate system. Lastly, several benchmark problems are examined by a computer program which has been written by the author in the MATLAB code.

2. Element formulation

2.1. Geometry of the solid shell element

The coordinates of a typical point in the eight node solid-shell element (Fig. 1) can be written as

$$x = \sum_{k=1}^{4} N_k \Big(\frac{1+\zeta}{2} x_k^t + \frac{1-\zeta}{2} x_k^b \Big) \tag{2.1}$$

where $N_k = N_k(\xi, \eta)$ are the two-dimensional isoparametric shape functions, $\boldsymbol{x} = [x, y, z]^\top$ are the position vectors; ξ, η and ζ are curvilinear coordinates. Here ξ, η and ζ are assumed to vary from -1 and $+1$.

The displacement field $\boldsymbol{u} = [u, v, w]^\top$ in the shell element can be approximated by

$$\boldsymbol{u} = \sum_{k=1}^{4} N_k \Big(\frac{1+\zeta}{2} \boldsymbol{u}_k^t + \frac{1-\zeta}{2} \boldsymbol{u}_k^b \Big) \tag{2.2}$$

where $\boldsymbol{u}_k = [u_k, v_k, w_k]^\top$ represents the displacement vector of node k.

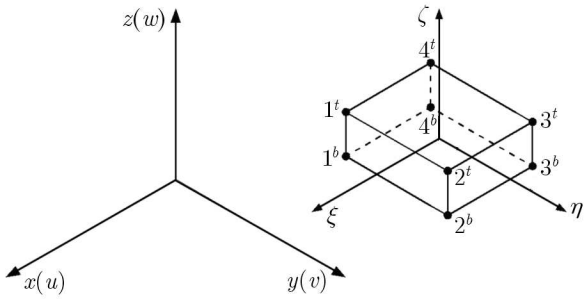

Fig. 1. Geometry of the eight-node solid-shell element

2.2. Straindisplacement relationships

The components of the displacement-based strain tensor $\boldsymbol{\varepsilon}^u$ in the natural set of coordinates (ξ, η, ζ) can be given as

$$\boldsymbol{\varepsilon}^u = [\varepsilon^u_{\xi\xi}, \varepsilon^u_{\eta\eta}, \varepsilon^u_{\zeta\zeta}, \varepsilon^u_{\xi\eta}, \varepsilon^u_{\xi\zeta}, \varepsilon^u_{\eta\zeta}]^\top \tag{2.3}$$

or

$$\boldsymbol{\varepsilon}^u = \mathbf{B}^u \boldsymbol{u} \qquad \boldsymbol{u} = [u_1, \ldots, u_k]^\top \qquad k = 1, \ldots, n \tag{2.4}$$

where $\mathbf{B}^u$ is the conventional strain-displacement matrix and $\boldsymbol{u}$ is the nodal displacement vector. The natural strain components defined in Eq. (2.3) can be determined (Sousa *et al.*, 2006) by using the displacement vector $\boldsymbol{u}$ and the covariant base vectors $\boldsymbol{g}_i$ as

$$\varepsilon^u_{\xi_i\xi_j} = \frac{1}{2}\Big(\frac{\partial \boldsymbol{u}}{\partial \xi_i}\boldsymbol{g}_j + \frac{\partial \boldsymbol{u}}{\partial \xi_j}\boldsymbol{g}_i\Big) \qquad \begin{matrix} i,j = 1,2,3 \\ \xi_2 = \eta \end{matrix} \qquad \begin{matrix} \xi_1 = \xi \\ \xi_3 = \zeta \end{matrix} \tag{2.5}$$

and

$$\boldsymbol{g}_i = \frac{\partial \boldsymbol{x}}{\partial \xi_i} \tag{2.6}$$

where $\boldsymbol{x}$ is the position vector.

The previously described strain field is related to the natural set of coordinates. Therefore, it is necessary to obtain the local physical strains from the natural strain components. The algorithm suggested by Valente (2004) is used for the transformation of the strains. It consists of the following five steps

$$\begin{aligned}
&a) \qquad \boldsymbol{r}^3 = \Big[\frac{\partial x}{\partial \xi}, \frac{\partial y}{\partial \xi}, \frac{\partial z}{\partial \xi}\Big]^\top \times \Big[\frac{\partial x}{\partial \eta}, \frac{\partial y}{\partial \eta}, \frac{\partial z}{\partial \eta}\Big]^\top \\
&b) \qquad \boldsymbol{r}^3 = \frac{\boldsymbol{r}^3}{\|\boldsymbol{r}^3\|} \\
&c) \qquad \boldsymbol{r}^1 = \Big[\frac{\partial x}{\partial \xi}, \frac{\partial y}{\partial \xi}, \frac{\partial z}{\partial \xi}\Big]^\top \\
&d) \qquad \boldsymbol{r}^1 = \frac{\boldsymbol{r}^1}{\|\boldsymbol{r}^1\|} \\
&e) \qquad \boldsymbol{r}^2 = \boldsymbol{r}^3 \times \boldsymbol{r}^1
\end{aligned}$$

Then, the components of direction cosines matrix $\widehat{\mathbf{T}}$ is

$$\widehat{\mathbf{T}} = [\boldsymbol{r}^1, \boldsymbol{r}^2, \boldsymbol{r}^3]^\top \mathbf{J}^{-1} \tag{2.7}$$

in which $\mathbf{J}$ is the conventional Jacobian matrix given by

$$\mathbf{J} = \begin{bmatrix} \dfrac{\partial x}{\partial \xi} & \dfrac{\partial y}{\partial \xi} & \dfrac{\partial z}{\partial \xi} \\ \dfrac{\partial x}{\partial \eta} & \dfrac{\partial y}{\partial \eta} & \dfrac{\partial z}{\partial \eta} \\ \dfrac{\partial x}{\partial \zeta} & \dfrac{\partial y}{\partial \zeta} & \dfrac{\partial z}{\partial \zeta} \end{bmatrix} \tag{2.8}$$

The natural and the local coordinate systems can be related by the second-order transformation tensor $\overline{\mathbf{T}}$

$$\overline{\mathbf{T}}=\begin{bmatrix} \widehat{T}_{11}\widehat{T}_{11} & \widehat{T}_{12}\widehat{T}_{12} & \widehat{T}_{13}\widehat{T}_{13} & \widehat{T}_{11}\widehat{T}_{12} & \widehat{T}_{11}\widehat{T}_{13} & \widehat{T}_{12}\widehat{T}_{13} \\ \widehat{T}_{21}\widehat{T}_{21} & \widehat{T}_{22}\widehat{T}_{22} & \widehat{T}_{23}\widehat{T}_{23} & \widehat{T}_{21}\widehat{T}_{22} & \widehat{T}_{21}\widehat{T}_{23} & \widehat{T}_{22}\widehat{T}_{23} \\ \widehat{T}_{31}\widehat{T}_{31} & \widehat{T}_{32}\widehat{T}_{32} & \widehat{T}_{33}\widehat{T}_{33} & \widehat{T}_{31}\widehat{T}_{32} & \widehat{T}_{31}\widehat{T}_{33} & \widehat{T}_{32}\widehat{T}_{33} \\ 2\widehat{T}_{11}\widehat{T}_{21} & 2\widehat{T}_{12}\widehat{T}_{22} & 2\widehat{T}_{13}\widehat{T}_{23} & \widehat{T}_{11}\widehat{T}_{22}+\widehat{T}_{12}\widehat{T}_{21} & \widehat{T}_{11}\widehat{T}_{23}+\widehat{T}_{21}\widehat{T}_{13} & \widehat{T}_{12}\widehat{T}_{23}+\widehat{T}_{22}\widehat{T}_{13} \\ 2\widehat{T}_{11}\widehat{T}_{31} & 2\widehat{T}_{12}\widehat{T}_{32} & 2\widehat{T}_{13}\widehat{T}_{33} & \widehat{T}_{11}\widehat{T}_{32}+\widehat{T}_{12}\widehat{T}_{31} & \widehat{T}_{11}\widehat{T}_{33}+\widehat{T}_{31}\widehat{T}_{13} & \widehat{T}_{12}\widehat{T}_{33}+\widehat{T}_{32}\widehat{T}_{13} \\ 2\widehat{T}_{21}\widehat{T}_{31} & 2\widehat{T}_{22}\widehat{T}_{32} & 2\widehat{T}_{23}\widehat{T}_{33} & \widehat{T}_{21}\widehat{T}_{32}+\widehat{T}_{22}\widehat{T}_{31} & \widehat{T}_{21}\widehat{T}_{33}+\widehat{T}_{31}\widehat{T}_{23} & \widehat{T}_{22}\widehat{T}_{33}+\widehat{T}_{32}\widehat{\mathbf{T}}_{23} \end{bmatrix} \tag{2.9}$$

2.3. Transverse shear locking treatment

In the pure displacement-based finite element formulation of shells, the employment of the full quadrature rules leads to locking effects related to transverse shear strain energy values. These formulations give unacceptable results, especially thickness values become smaller. To resolve the shear locking problem without reducing the quadrature rules, the ANS method is applied. The assumed transverse shear strains are based on the constant-linear interpolations of the compatible transverse shear strains $\varepsilon^u_{\xi\zeta}$ and $\varepsilon^u_{\eta\zeta}$ evaluated at the midpoints of the element edges. The local transverse shear strains are

$$\begin{Bmatrix} \overline{\varepsilon}^u_{xz} \\ \overline{\varepsilon}^u_{yz} \end{Bmatrix} = \begin{bmatrix} \overline{T}_{55} & \overline{T}_{56} \\ \overline{T}_{65} & \overline{T}_{66} \end{bmatrix} \begin{Bmatrix} \varepsilon^{ANS}_{\xi\zeta} \\ \varepsilon^{ANS}_{\eta\zeta} \end{Bmatrix} \tag{2.10}$$

in which the interpolated natural transverse shear strains are given by

$$\begin{Bmatrix} \varepsilon^{ANS}_{\xi\zeta} \\ \varepsilon^{ANS}_{\eta\zeta} \end{Bmatrix} = \begin{Bmatrix} (1-\eta)\varepsilon^u_{\xi\zeta}|_{(0,-1,0)} + (1+\eta)\varepsilon^u_{\xi\zeta}|_{(0,1,0)} \\ (1-\xi)\varepsilon^u_{\eta\zeta}|_{(-1,0,0)} + (1+\xi)\varepsilon^u_{\eta\zeta}|_{(1,0,0)} \end{Bmatrix} \tag{2.11}$$

2.4. Trapezoidal locking treatment

Trapezoidal locking occurs in the case of curved geometry. To resolve the locking effect from the parasitic transverse normal strain, we interpolate the natural transverse normal strain at the nodal directors. That is

$$\varepsilon^{ANS}_{\zeta\zeta} = N_1\varepsilon^u_{\zeta\zeta}\Big|_{(-1,-1,0)} + N_2\varepsilon^u_{\zeta\zeta}\Big|_{(1,-1,0)} + N_3\varepsilon^u_{\zeta\zeta}\Big|_{(1,1,0)} + N_4\varepsilon^u_{\zeta\zeta}\Big|_{(-1,1,0)} \tag{2.12}$$

and the local transverse normal strain is

$$\overline{\varepsilon}^u_{zz} = \overline{T}_{33}\varepsilon^{ANS}_{\zeta\zeta} \tag{2.13}$$

2.5. Membrane and thickness locking treatment

To avoid the membrane and thickness locking problems in the solid shell formulations, the displacement-based strain field related to the membrane strains $(\varepsilon^u_{\xi\xi}, \varepsilon^u_{\eta\eta}, \varepsilon^u_{\xi\eta})$ and the transverse normal strain $\varepsilon^u_{\zeta\zeta}$ can be improved using the EAS method as following

$$\boldsymbol{\varepsilon} = \boldsymbol{\varepsilon}^u + \boldsymbol{\varepsilon}^\alpha \tag{2.14}$$

where $\boldsymbol{\varepsilon}$ is the improved strain field and $\boldsymbol{\varepsilon}^\alpha$ is the additive enhanced strain field. The additive enhanced strain field can be rewritten as

$$\boldsymbol{\varepsilon}^\alpha = \mathbf{B}^\alpha \boldsymbol{\alpha} \qquad \boldsymbol{\alpha} = [\alpha_1, \alpha_2, \cdots, \alpha_7]^\top \tag{2.15}$$

where $\mathbf{B}^\alpha$ and is the EAS-based strain-displacement matrix, $\boldsymbol{\alpha}$ is the vector of EAS variables. The matrix is given by

$$\mathbf{B}^\alpha = \begin{bmatrix} \xi & 0 & 0 & 0 & 0 & 0 & 0 \\ 0 & \eta & 0 & 0 & 0 & 0 & 0 \\ 0 & 0 & \zeta & \xi\zeta & \eta\zeta & 0 & 0 \\ 0 & 0 & 0 & 0 & 0 & \xi & \eta \\ 0 & 0 & 0 & 0 & 0 & 0 & 0 \\ 0 & 0 & 0 & 0 & 0 & 0 & 0 \end{bmatrix} \tag{2.16}$$

In order to pass the membrane patch test and out-of-plane bending patch test, the bilinear polynomials for the transverse normal strain $\varepsilon_{\zeta\zeta}$ are necessary, i.e. the minimum number of EAS parameters for $\varepsilon_{\zeta\zeta}$ should be three. In addition, without a combination with the ANS method to remedy the shear-locking problem, even the 30-parameter EAS element cannot pass the out-of-plane bending patch test (Vu-Quoc and Tan, 2003). The enhanced strain field $\boldsymbol{\varepsilon}^\alpha$ in Eq. (2.16) is transformed into local coordinates by Eq. (2.9)

$$\overline{\varepsilon}^\alpha = \frac{\det \mathbf{J}_0}{\det \mathbf{J}} \overline{\mathbf{T}}_0 \boldsymbol{\varepsilon}^\alpha = \mathbf{B}^\alpha \boldsymbol{\alpha} \tag{2.17}$$

where $\overline{\mathbf{T}}_0$ are evaluated at the element center. The local membrane strains can be given in the form of

$$\begin{Bmatrix} \overline{\varepsilon}^u_{xx} \\ \overline{\varepsilon}^u_{yy} \\ \overline{\varepsilon}^u_{xy} \end{Bmatrix} = \begin{bmatrix} \overline{T}_{11} & \overline{T}_{12} & \overline{T}_{14} \\ \overline{T}_{21} & \overline{T}_{22} & \overline{T}_{24} \\ \overline{T}_{41} & \overline{T}_{42} & \overline{T}_{44} \end{bmatrix} \begin{Bmatrix} \varepsilon^u_{\xi\xi} \\ \varepsilon^u_{\eta\eta} \\ \varepsilon^u_{\xi\eta} \end{Bmatrix} \tag{2.18}$$

2.6. Co-rotational formulation

The initial local system coordinates $\boldsymbol{X}_L^k$ of the node k can be given as

$$\boldsymbol{X}_L^k = \boldsymbol{X}^k - \boldsymbol{X}^1 \tag{2.19}$$

It is considered that the initial coordinates in the local and global systems are the same.

To obtain the local axes within the nonlinear process, it is necessary to determine the rotation matrix $\mathbf{R}$. The incremental global deformation gradient $\boldsymbol{F}$ computed at the center of the element can be written as

$$\boldsymbol{F} = \mathbf{R}\mathbf{U} \tag{2.20}$$

where $\mathbf{U}$ is the right stretch tensor. The rotation matrix can be evaluated from the well-known polar decomposition theorem, mostly with the determination of eigenvalues of the right Cauchy-Green tensor.

Thus, the rotation matrix $\mathbf{R}$ is

$$\mathbf{R} = [\boldsymbol{e}_1, \boldsymbol{e}_2, \boldsymbol{e}_3] \tag{2.21}$$

where $\boldsymbol{e}_1$, $\boldsymbol{e}_2$ and $\boldsymbol{e}_3$ are the local rotated unit vectors. The relationship between the local and global current position vectors of the node k is explicitly given by

$$\boldsymbol{x}_L^k = \boldsymbol{X}^k + \boldsymbol{u}_L^k = \begin{Bmatrix} X_L \\ Y_L \\ Z_L \end{Bmatrix}^k + \begin{Bmatrix} u_L \\ v_L \\ w_L \end{Bmatrix}^k = \mathbf{R}^\top (\boldsymbol{x}_G^k - \boldsymbol{x}_G^1) = \mathbf{R}^\top \boldsymbol{x}_G^{k1} \tag{2.22}$$

where $\boldsymbol{x}_L^k$ and $\boldsymbol{x}_G^k$ are the current coordinates for the local and global position vectors for the node k, respectively.

The differentiation of Eq. (2.22) gives the relationship between the variation of the local displacements and the variation of the global displacements

$$\delta \boldsymbol{u}_L^k = \mathbf{R}^\top \delta \boldsymbol{u}_G^k + \delta \mathbf{R}^\top \boldsymbol{x}_G^{k1} \tag{2.23}$$

We can rewrite Eq. (2.23) using a skew-symmetric matrix $\mathbf{S}$

$$\begin{aligned} \mathbf{S}(\boldsymbol{x}_G^{k1}) &= \begin{bmatrix} 0 & -z_G^{k1} & y_G^{k1} \\ z_G^{k1} & 0 & -x_G^{k1} \\ -y_G^{k1} & -x_G^{k1} & 0 \end{bmatrix} \\ \delta \boldsymbol{u}_L^k &= \mathbf{R}^\top \delta \boldsymbol{u}_G^k + \mathbf{R}^\top \mathbf{S}(\boldsymbol{x}_G^{k1}) \delta \boldsymbol{\theta} \end{aligned} \tag{2.24}$$

we can rewrite Eq. $(2.24)_2$ at the element level as

$$\delta \boldsymbol{u}_L = [\operatorname{diag} \mathbf{R}^\top]\delta \boldsymbol{u}_G + [\operatorname{col}(\mathbf{R}^\top \mathbf{S}(\boldsymbol{x}_G^{k1}))]\delta\boldsymbol{\theta} \tag{2.25}$$

where $\delta\boldsymbol{\theta}$ is a pseudo-vector. To find an expression for the pseudo-vector $\delta\boldsymbol{\theta}$, we can write a spin vector $\boldsymbol{\Omega}$ using local quantities

$$\boldsymbol{\Omega} = \begin{bmatrix} \dfrac{\partial u_L}{\partial Y_L} - \dfrac{\partial v_L}{\partial X_L} \\ \dfrac{\partial u_L}{\partial Z_L} - \dfrac{\partial w_L}{\partial X_L} \\ \dfrac{\partial v_L}{\partial Z_L} - \dfrac{\partial w_L}{\partial Y_L} \end{bmatrix} = \mathbf{A}_L^\top \boldsymbol{u}_L = \mathbf{0} \tag{2.26}$$

where $\mathbf{A}_L$ is the 24×3 matrix. Differentiating this spin vector, we can get

$$\begin{aligned} &\delta\boldsymbol{\Omega} = \mathbf{A}_L^\top \delta \boldsymbol{u}_L = \mathbf{A}_L^\top [\operatorname{diag} \mathbf{R}^\top]\delta \boldsymbol{u}_G + \mathbf{A}_L^\top [\operatorname{col}(\mathbf{R}^\top \mathbf{S}(\boldsymbol{x}_G^{k1}))]\delta\boldsymbol{\theta} = \mathbf{0} \\ &\delta\boldsymbol{\theta} = -[\mathbf{A}_L^\top \operatorname{col}(\mathbf{R}^\top \mathbf{S}(x_G^{k1}))]^{-1} \mathbf{A}_L^\top [\operatorname{diag} \mathbf{R}^\top]\delta \boldsymbol{u}_G = \mathbf{V}^\top \delta \boldsymbol{u}_G \end{aligned} \tag{2.27}$$

Consequently, using Eq. (2.25) and Eq. $(2.27)_2$

$$\delta \boldsymbol{u}_L = [\operatorname{diag} \mathbf{R}^\top + \operatorname{col}(\mathbf{R}^\top \mathbf{S}(x_G^{k1}))\mathbf{V}^\top]\delta \boldsymbol{u}_G = \mathbf{T}\delta \boldsymbol{u}_G \tag{2.28}$$

where $\mathbf{T}$ is the transformation matrix.

2.7. Tangent stiffness matrix

The local internal force vector $\boldsymbol{F}_{i,L}$ of the 8-node solid-shell element can be determined by

$$\boldsymbol{F}_{i,L} = \int \mathbf{B}_L^u \boldsymbol{\sigma}_L \, dV_0 \tag{2.29}$$

where $\mathbf{B}_L^u$ is the strain-displacement matrix, $\boldsymbol{\sigma}_L$ is the local stress vector. The relationship between the global and local internal force vectors can be given as

$$\boldsymbol{F}_{i,G} = \mathbf{T}^\top \boldsymbol{F}_{i,L} = \mathbf{T}^\top \mathbf{K}_L \boldsymbol{u}_L \tag{2.30}$$

where $\mathbf{K}_L$ is the linear local stiffness matrix. The global tangent stiffness matrix $\mathbf{K}_T$ can be determined by differentiation of Eq. (2.30) such as

$$\delta \boldsymbol{F}_{i,G} = \mathbf{T}^\top \delta \boldsymbol{F}_{i,L} + \delta \mathbf{T}^\top \boldsymbol{F}_{i,L} = (\mathbf{T}^\top \mathbf{K}_L \mathbf{T} + \mathbf{K}_{\sigma 1})\delta \boldsymbol{u}_G = \mathbf{K}_T \delta \boldsymbol{u}_G \tag{2.31}$$

where $\mathbf{K}_{\sigma 1}$ is the initial stress matrix. This matrix can be determined using variation of the transformation matrix $\mathbf{T}$

$$\delta \mathbf{T}^\top \boldsymbol{F}_{i,L} = \delta[\operatorname{diag} \mathbf{R}^\top + \operatorname{col}(\mathbf{R}^\top \mathbf{S}(\boldsymbol{x}_G^{k1}))\mathbf{V}^\top]\boldsymbol{F}_{i,L} = \mathbf{K}_{\sigma 1}\delta \boldsymbol{u}_G \tag{2.32}$$

If we define the local internal force vector $\widetilde{\boldsymbol{F}}^k_{i,L}$ for the node k such as

$$\widetilde{\boldsymbol{F}}^k_{i,L} = \mathbf{R}\boldsymbol{F}^k_{i,L} \tag{2.33}$$

then the initial stress matrix $\mathbf{K}_{\sigma 1}$ can take the form

$$\mathbf{K}_{\sigma 1} = -\operatorname{col}(\mathbf{S}(\widetilde{\boldsymbol{F}}^k_{i,L}))\mathbf{V}^\top + \mathbf{V}\operatorname{row}(\mathbf{S}(\widetilde{\boldsymbol{F}}^k_{i,L})) + \mathbf{V}\operatorname{row}(\mathbf{S}(\boldsymbol{x}^{k1}_G))\operatorname{col}(\mathbf{S}(\widetilde{\boldsymbol{F}}^k_{i,L}))\mathbf{V}^\top \tag{2.34}$$

however, the last term in Eq. (2.34) produces a non-symmetric matrix. The non-symmetric part can be written as

$$\text{Non} - \text{ sym } = \frac{1}{2}\sum_{k=1}^{n}(\boldsymbol{x}^{k1}_G\widetilde{\boldsymbol{F}}^{kT}_{i,L} - \widetilde{\boldsymbol{F}}^k_{i,L}\boldsymbol{x}^{k1T}_G) \tag{2.35}$$

Then, the initial stress matrix $\mathbf{K}_{\sigma 1}$ is given by

$$\mathbf{K}_{\sigma 1} = -\operatorname{col}(\mathbf{S}(\widetilde{\boldsymbol{F}}^k_{i,L}))\mathbf{V}^\top + \mathbf{V}\operatorname{row}(\mathbf{S}(\widetilde{\boldsymbol{F}}^k_{i,L})) + \mathbf{V}\operatorname{sym}\Big(\sum_{k=1}^{n}\mathbf{S}(\boldsymbol{x}^{k1}_G)\mathbf{S}(\widetilde{\boldsymbol{F}}^k_{i,L})\Big)\mathbf{V}^\top \tag{2.36}$$

As a result, we can write the stiffness matrices used in the incremental-iterative procedure in the matrix form as

$$\begin{aligned} \mathbf{K}^{uu} &= \int_V \overline{\mathbf{B}}^{u\top}_L \mathbf{D}\overline{\mathbf{B}}^u_L \, dV_0 \qquad & \mathbf{K}^{u\alpha} &= \int_V \overline{\mathbf{B}}^{u\top}_L \mathbf{D}\overline{\mathbf{B}}^\alpha_L \, dV_0 \\ \mathbf{K}^{\alpha\alpha} &= \int_V \overline{\mathbf{B}}^{\alpha\top}_L \mathbf{D}\overline{\mathbf{B}}^\alpha_L \, dV_0 \end{aligned} \tag{2.37}$$

where $\mathbf{D}$ is the symmetric 6×6 material matrix.

The EAS parameters $\boldsymbol{\alpha}$ can be eliminated at the element level as follows

$$\begin{aligned} \delta\boldsymbol{\alpha} &= (\mathbf{K}^{\alpha\alpha})^{-1}(\mathbf{K}^{u\alpha\top}\delta\boldsymbol{u}_G - \boldsymbol{F}^\alpha_{i,L}) \qquad & \overline{\boldsymbol{F}}_{i,L} &= \boldsymbol{F}_{i,L} - \mathbf{K}^{u\alpha}(\mathbf{K}^{\alpha\alpha})^{-1}\boldsymbol{F}^\alpha_{i,L} \\ \mathbf{K}_L &= \mathbf{K}^{uu} - \mathbf{K}^{u\alpha}(\mathbf{K}^{\alpha\alpha})^{-1}\mathbf{K}^{u\alpha\top} & \mathbf{K}_T &= \mathbf{T}^\top\mathbf{K}_L\mathbf{T} + \mathbf{K}_{\sigma 1} \end{aligned} \tag{2.38}$$

where $\mathbf{K}_T$ is the tangent stiffness matrix. Then, we can determine the out-of-balance force $\boldsymbol{P}$ used in the nonlinear procedure as

$$\boldsymbol{P} = \boldsymbol{F}_e - \mathbf{T}^\top\overline{\boldsymbol{F}}_{i,L} \tag{2.39}$$

where $\boldsymbol{F}_e$ is the external force.

2.8. The solution method

In order to compute the nodal displacements, the load controlled Newton-Raphson method and the spherical arc-length algorithm with the predictor criterion of Feng *et al.* (1995, 1996) are used. The convergence criterion is chosen as

$$\|\delta \boldsymbol{u}_G\| < 10^{-5} \|\Delta u_G\| \tag{2.40}$$

where δ and Δ parameters indicate the iterative and incremental quantities, respectively.

3. Numerical examples

The element stiffness matrix is computed numerically using a $2 \times 2 \times 2$ Gauss integration scheme. Most of the results presented here are compared with the solutions of Sze *et al.* (2004) who chosen the S4R element in their analysis and SHELL63 element of ANSYS.

3.1. A cantilever subjected to an end shear force

A cantilever is subjected to an end shear force F, shown in Fig. 2. The problem is examined using 20×1 enhanced solid-shell elements. Figure 3 plots the end shear force against the vertical and horizontal tip displacements of the present, 16×1 S4R and SHELL63 element results. The differences between three analyses are almost indistinguishable.

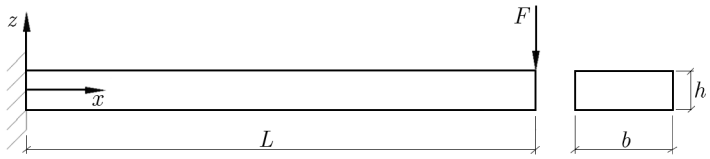

Fig. 2. Figure 2. Cantilever subjected to end shear force; $E = 1.2 \cdot 10^6$, $\nu = 0$, $L = 10$, $b = 1$, $h = 0.1$, $F = 4$

3.2. Buckling of a beam under an axial compressive load

An isotropic beam is subjected to a compressive load F, shown in Fig. 4. The compressive load is applied with an imperfect angle θ of 0.0573° to activate the buckling behavior of the beam. The critical load calculated by Euler's formula is $F_{cr} = 1124.21$. Figure 5 plots the compressive force against the

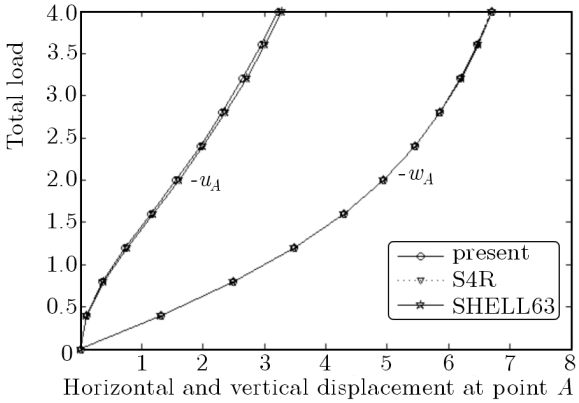

Fig. 3. Loaddisplacement curves for cantilever subjected to end shear force

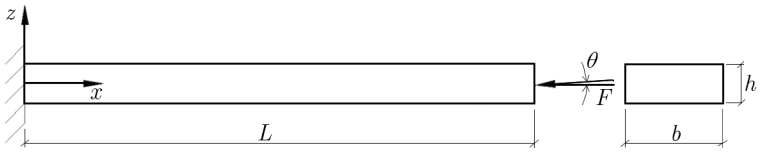

Fig. 4. Cantilever subjected to compressive force; $E = 2 \cdot 10^{11}$, $\nu = 0.3$, $L = 0.5$, $b = 0.075$, $h = 0.0045$

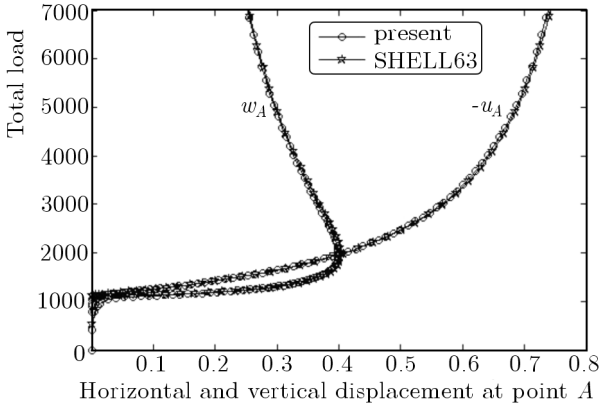

Fig. 5. Loaddisplacement curves for cantilever subjected to compressive force

vertical and horizontal tip displacements of the point A, and the SHELL63 element results are also given in the same figure. In addition, the detailed portion of Fig. 5 related with the critical buckling load is given in Fig. 6. The present and reference solutions are very close to each other.

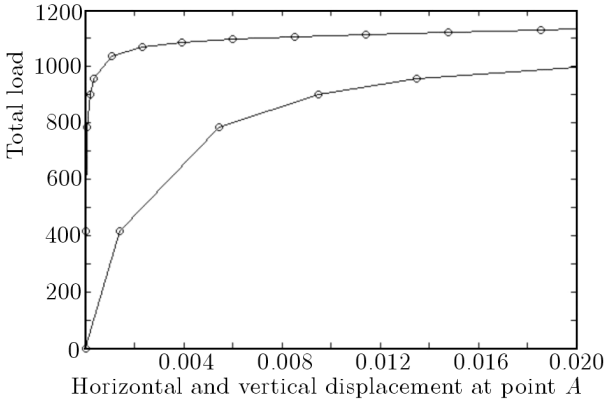

Fig. 6. Detailed portion of Fig. 5 related with critical buckling load

3.3. Hinged semi-cylindrical roof

This is a commonly used benchmark problem for large-displacement analysis of a shallow shell subjected to a central pinching force, see Fig. 7. The

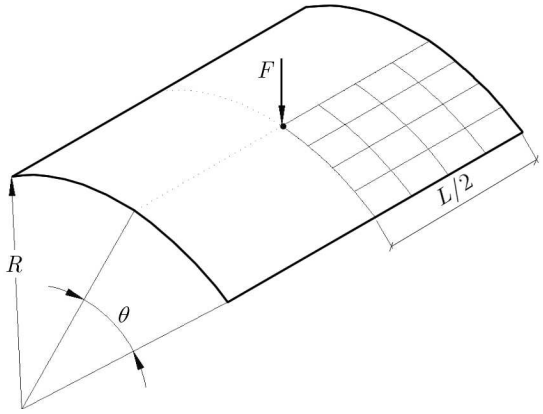

Fig. 7. Hinged semi-cylindrical roof subjected to central point load; $E = 3102.75$, $\nu = 0.3$, $R = 2540$, $L = 508$, $h = 12.7$ or $h = 6.35$, $\theta = 0.1$

problem was studied by many researchers (Chroscielewski *et al.*, 1992; Ibrahimbegovic and Frey, 1994; Kreja *et al.*, 1997; Sousa *et al.*, 2006). The straight edges are hinged and immovable, while the curved edges are free. The structure is modeled with 10×10 enhanced solid-shell elements on one quarter of its surface and with two elements in the thickness direction. We investigate the buckling behavior of the cylindrical shell for two different thicknesses. The vertical displacements of the point A are reproduced in Fig. 8 and 9, plotted

against the load level and compared to the S4R and SHELL63 element solutions. A very good agreement between the solutions along the entire unstable loaddisplacement path is noticeable.

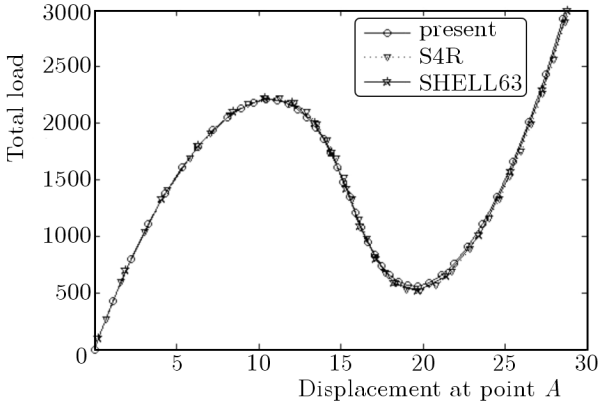

Fig. 8. Loaddisplacement curves for hinged semi-cylindrical roof for thickness $h = 12.7$

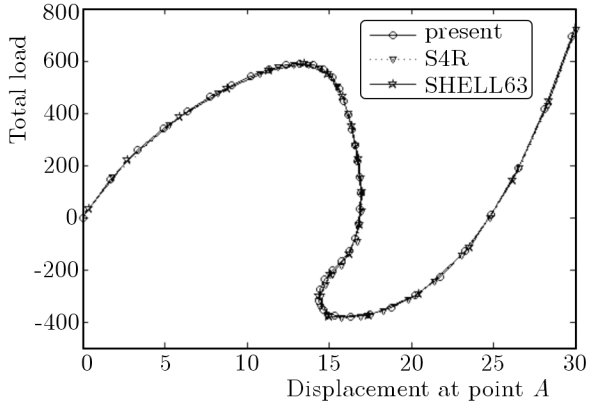

Fig. 9. Loaddisplacement curves for hinged semi-cylindrical roof for thickness $h = 6.35$

3.4. Pull-out of an open cylinder

A cylinder is pinched by two radially pulling forces F as shown in Fig. 10. The problem was analyzed by many researchers (Sansour and Bednarczyk, 1995; Valen, 2004; Witkowski, 2009). Both ends of the cylinder are free. One quarter of the cylinder is discretized and the corresponding symmetry is taken into account. The structure is modeled with 24×36 enhanced solid-shell

elements. The results are shown in Figure 11 which presents the radial displacement of the points A, B and C with respect to the magnitude of the applied forces.

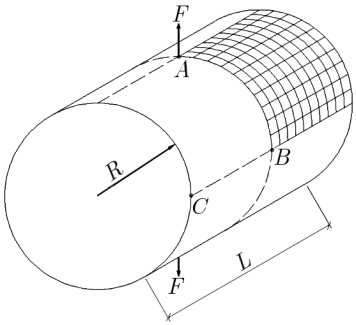

Fig. 10. Pull-out of open cylinder; $E = 10.5 \cdot 10^6$, $\nu = 0.3$, $R = 4.953$, $L = 10.35$, $h = 0.094$

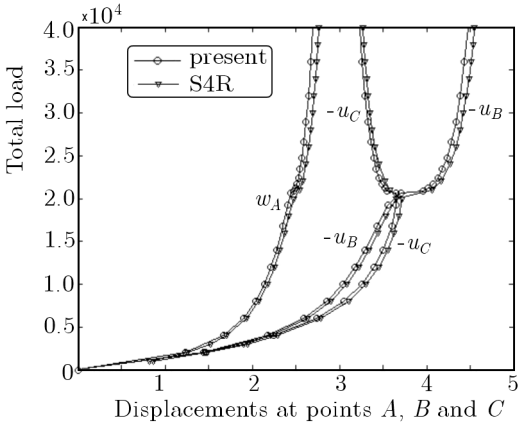

Fig. 11. Loaddisplacement curves for open cylinder

4. Conclusions

A nearly locking-free formulation of an 8-node solid-shell element based on the co-rotational description of motion was developed. The ANS and the EAS approaches were used to alleviate the locking problems. The polar decomposition theorem was employed to obtain the rotation matrix and the transformation matrix which defines the relationship between the variations of local displacements. Furthermore, the variation of the global displacements was also

formulated. Thus, geometric nonlinearities were taken into account via rotation of the local system. The analyzed benchmark problems showed that the proposed method is reliable and effective. Moreover, it is easy to implement.

References

1. Andelfinger U., Ramm E., 1993, EAS-elements for two-dimensional, three-dimensional, plate and shell structures and their equivalence to HR-elements, *International Journal for Numerical Methods in Engineering*, **36**, 1311-1337
2. Argyris J.H., Bahner H., Doltsnis J., et al., 1979, Finite element method – the natural approach, *Computer Methods in Applied Mechanics and Engineering*, **17/18**, l-106
3. Bathe K.J., Dvorkin E.N., 1986, A formulation of general shell elements – The use of mixed interpolation of tensorial components, *International Journal for Numerical Methods in Engineering*, **22**, 697-722
4. Belytschko T., Glaum L.W., 1979, Application of higher order corotational stretch theories to nonlinear finite element analysis, *Computers and Structures*, **10**, 175-182
5. Bucalem M.L., Bathe K.J., 1993, Higher-order MITC general shell elements, *International Journal for Numerical Methods in Engineering*, **36**, 3729-3754
6. Chroscielewski J., Makowski J., Stumpf H., 1992, Genuinely resultant shell finite elements accounting for geometric and material non-linearity, *International Journal for Numerical Methods in Engineering*, **35**, 6394
7. Crisfield M.A., Moita G.F., 1996, A co-rotational formulation for 2-D continua including incompatible modes, *International Journal of Numerical Methods in Engineering*, **39**, 2619-2633
8. Felippa C.A., Haugen B., 2005, A unified formulation of small strain corotational finite elements: I. Theory, *Computer Methods in Applied Mechanics and Engineering*, **194**, 2285-2335
9. Feng Y.T., Peric D., Owen D.R.J., 1995, Determination of travel directions in path-following methods, *Mathematical and Computer Modelling*, **21**, 43-59
10. Feng Y.T., Peric D., Owen D.R.J., 1996, A new criterion for determination of initial loading parameter in arc-length methods, *Computers and Structures*, **58**, 479-485
11. Fontes Valente R.A., 2004, *Developments on Shell and Solid-Shell Finite Elements Technology in Nonlinear Continuum Mechanics*, Ph.D. Thesis, University of Porto, Portugal

12. Harnau M., Schweizerhof K., 2002, About linear and quadratic "solid-shell" elements at large deformations, *Computers and Structures*, **80**, 805-817

13. Hauptmann R., Schweizerhof K., 1998, A systematic development of "solid-shell" element formulations for linear and non-linear analyses employing only displacement degrees of freedom, *International Journal for Numerical Methods in Engineering*, **42**, 49-69

14. Hauptmann R., Scheizerhof K., Doll S., 2000, Extension of the "solid-shell" concept for application to large elastic and large elastoplastic deformations, *International Journal for Numerical Methods in Engineering*, **49**, 1121-1141

15. Hughes T.J.R., Cohen M., Haroun M., 1978, Reduced and selective integration techniques in the finite element analysis of plates, *Nuclear Engineering and Design*, **46**, 203-222

16. Hughes T.J.R., Taylor R.L., Kanoknukulchai W., 1977, A simple and efficient finite element for plate bending, *International Journal for Numerical Methods in Engineering*, **11**, 1529-1543

17. Ibrahimbegovic A., Frey F., 1994, Stress resultant geometrically nonlinear shell theory with drilling rotations – Part II: Computational aspects, *Computer Methods in Applied Mechanics and Engineering*, **118**, 285-308

18. Klinkel S., Wagner W., 1997, A geometrical non-linear brick element, *International Journal for Numerical Methods in Engineering*, **40**, 4529-4545

19. Kreja I., Schmidt R., Reddy J.N., 1997. Finite elements based on a first-order shear deformation moderate rotation shell theory with applications to the analysis of composite structures, *International Journal of Non-Linear Mechanics*, **32**, 11231142

20. Miehe C., 1998, Theoretical and computational model for isotropic elastoplastic stress analysis in shells at large strains, *Computer Methods in Applied Mechanics and Engineering*, **155**, 193-233

21. Moita G.F., Crisfield M.A., 1996, A finite element formulation for 3-D continua using the co-rotational technique, *International Journal of Numerical Methods in Engineering*, **39**, 3775-3792

22. Panasz P., Wisniewski K., 2008, Nine-node shell elements with 6 dofs/node based on two-level approximations. Part I Theory and linear tests, *Finite Elements in Analysis and Design*, **44**, 784796

23. Sansour C., Bednarczyk H., 1995, The Cosserat surface as a shell model, theory and finite-element formulation, *Computer Methods in Applied Mechanics and Engineering*, **120**, 132

24. Simo J.C., Rifai M.S., 1990, A class of mixed assumed strain methods and the method of incompatible modes, *International Journal for Numerical Methods in Engineering*, **29**, 1595-1638

25. Sousa R.J.A., Cardoso R.P.R., Fontes Valente R.A., Yoon Y.W., Gracio J.J., Natal Jorge R.M., 2004, A new one-point quadrature Enhanced Assumed Strain (EAS) solid-shell element with multiple integration points along thickness. Part I – Geometrically linear applications, *International Journal of Numerical Methods in Engineering*, **62**, 952-977

26. Sousa R.J.A., Cardoso R.P.R., Fontes Valente R.A., Yoon Y.W., Gracio J.J., Natal Jorge R.M., 2006. A new one-point quadrature Enhanced Assumed Strain solid-shell element with multiple integration points along thickness. Part II - Nonlinear applications, *International Journal of Numerical Methods in Engineering*, **67**, 160-188

27. Sze K.Y., Liu X.H., Lo S.H., 2004, Popular benchmark problems for geometric nonlinear analysis of shells, *Finite Elements in Analysis and Design*, **40**, 1551-1569

28. Sze K.Y., Yao L.Q., 2000, A hybrid stress ANS solid-shell element and its generalization for smart structure modelling. Part I: Solid-shell element formulation, *International Journal of Numerical Methods in Engineering*, **48**, 545-564

29. Sze K.Y., Yao L.Q., Yi S., 2000, A hybrid stress ANS solid-shell element and its generalization for smart structure modelling. Part II: Smart structure modelling, *International Journal of Numerical Methods in Engineering*, **48**, 565-582

30. Tan X.G., Vu-Quoc L., 2005, Optimal solid shell element for large deformable composite structures with piezoelectric layers and active vibration control, *International Journal of Numerical Methods in Engineering*, **64**, 1981-2013

31. Urthaler Y., Reddy J.N., 2005, A corotational finite element formulation for the analysis of planar beams, *Communications in Numerical Methods in Engineering*, **21**, 553-570

32. Vu-Quoc L., Tan X.G., 2003, Optimal solid shells for non-linear analyses of multilayer composites. I Statics, *Computer Methods in Applied Mechanics and Engineering*, **192**, 975-1016

33. Wempner G., 1969, Finite elements, finite rotations and small strains of flexible shells, *The International Journal of Solids and Structures*, **5**, 117-153

34. Witkowski W., 2009, 4-Node combined shell element with semi-EAS-ANS strain interpolations in 6-parameter shell theories with drilling degrees of freedom, *Computational Mechanics*, **43**, 307319

35. Zienkiewicz O.C., Taylor R.L., Too J.M., 1971, Reduced integration techniques in finite element method, *International Journal for Numerical Methods in Engineering*, **3**, 275-290

Współrotacyjny opis bryłowo-powłokowego elementu skończonego oparty na metodzie założonych (ANS) i poszerzonych (EAS) odkształceń

Streszczenie

W pracy zaprezentowano opis ośmiowęzłowego bryłowo-powłokowego elementu skończonego. W celu osłabienia tzw. efektu blokady zastosowano metody założonych (ANS) i poszerzonych (EAS) odkształceń. Do opisu elementu zaadoptowano sformułowanie współrotacyjne, co pozwoliło na uwzględnienie nieliniowości poprzez obrót lokalnego układu współrzędnych. Przedstawiono także kilka zagadnień sprawdzających (zadań progowych) dla demonstracji efektywności tak zdefiniowanego elementu skończonego.

Manuscript received November 23, 2009; accepted for print March 1, 2010